Chapter 7
Pros and Cons on Magnetic Nanoparticles Use in Biomedicine and Biotechnologies Applications

Florina M. Bojin and Virgil Paunescu

Abstract In recent years, the design and synthesis of colloidal magnetic suspensions have attracted an increased interest especially in the fields of biotechnology and biomedicine because they have many applications including targeted drug delivery, cell labeling and magnetic cell separation, hyperthermia, tissue repairing, magnetic resonance imaging (MRI) contrast enhancement, enzyme immobilization, immunoassays, protein purification, etc.

7.1 Introduction

Magnetic nanoparticles (MNPs) used in biomedicine must meet several requirements. They have to be non-toxic, chemically stabile, uniform in size, well stabilized under physiological conditions, biocompatible and to present high magnetization. Magnetite (Fe_3O_4) and maghemite (γ-Fe_2O_3) are the most suitable iron oxide nanoparticles employed for biomedical applications because they are biocompatible, have low toxicity in the human body and show a superparamagnetic behavior.

Therefore, synthesis of magnetic iron oxide nanoparticles with tailored properties has attracted considerable scientific and technological interest. Various synthesis routes were developed for producing magnetic particles, such as co-precipitation, microemulsion method, thermal decomposition of different organic precursors, spray pyrolysis, and sol-gel method.

For biomedical applications, magnetic iron oxide nanoparticles must be dispersed in biocompatible media in order to obtain stable colloidal suspensions. In order to prevent the particle aggregation and to improve the biocompatibility and stability, nanoparticles are coated with various surfactants: poly(ethylene glycol),

F.M. Bojin (✉) • V. Paunescu
Department of Functional Sciences, "Victor Babes" University of Medicine and Pharmacy Timisoara, Etimie Murgu Square No. 2A, 300041 Timisoara, Romania
e-mail: florinabojin@umft.ro

M. Lungu et al. (eds.), *Nanoparticles' Promises and Risks*,
DOI 10.1007/978-3-319-11728-7_7

oleic acid, poly(acrylic acid), gluconic acid, other polymers, liposome and fatty acids.

We investigated the influence of colloidal suspensions of magnetic iron oxide nanoparticles on tumor and normal (adult bone marrow-derived mesenchymal stem cells (MSCs)) cell lines cultivated in vitro conditions. Magnetite nanoparticles were prepared by combustion synthesis as well by co-precipitation route. Combustion synthesized Fe_3O_4 nanoparticles proved to be superior to the co-precipitated magnetite nanoparticles in terms of cell viability. The influence of different concentrations on MNPs on cellular morphology, ultrastructure expression of phenotypical markers, and viability were examined in order to establish whether the combustion synthesized nanoparticles may be used for in vitro and in vivo applications. Tumor cells treated with combustion synthesized nanoparticles had a lower viability when compared to similar cells treated with co-precipitated nanoparticles. When treated with combustion synthesized nanoparticles, tumor cells were enucleated and lost their adhesion abilities. Normal cells treated with combustion synthesized nanoparticles developed anchorage structures, which made them more resistant to the chemical stress. This remarkable behavior of combustion synthesized Fe_3O_4 nanoparticles opens a whole new perspective on using the combustion synthesized magnetite nanoparticles in cancer therapy due to their selective intrinsic behavior.

7.2 Theoretical Study

7.2.1 Magnetic Nanoparticles. General Considerations

Magnetic materials can be considered indispensable for modern technology. They can enter in composition of different electronic devices and appliances and are intensely used in industrial and medical equipment.

The ferromagnetic and ferrimagnetic materials with nanometric dimensions present a magnetism form called superparamagnetism. This involves smaller than 20 nm dimensions of the particles. Superparamagnetic materials present a single magnetic domain and do not present hysteresis [1–4]. In case that the particle dimension is increasing above one critical size, which depends on the nature of the material, it becomes multi-domain. The most used magnetic material is magnetite, Fe_3O_4 and or maghemite—γ-Fe_2O_3 [5, 6].

Magnetite is a natural mineral that presents a crystalline structure of inversed spinel (Fig. 7.1) with a cubic cellular unit with the central sides constituted from 56 atoms: 32 O^{2-} anions, 16 Fe^{3+} cations, and 8 Fe^{2+} cations.

In the spinel inverse structure of Fe_3O_4, half of the F^{3+} ions are tetrahedrally coordinated being surrounded by four oxygen atoms, and the other half of the F^{3+} ions and all Fe^{2+} ions are octahedral coordinated [8, 9].

Magnetite is oxidized at maghemite rapidly in air which is also ferromagnetic but has a slightly reduced magnetic response. This process occurs only at the

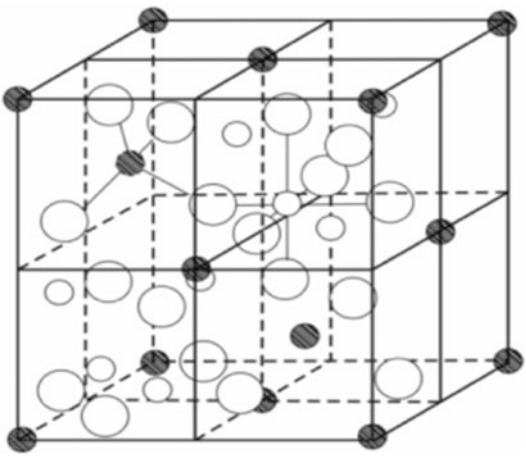

Fig. 7.1 Inversed spinel structure of magnetite [7]

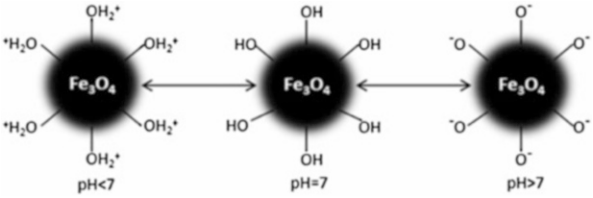

Fig. 7.2 Behavior of the magnetite particle according to the acid or basic pH [11]

surface of the crystals. The center of the crystals is also oxidized, by the diffusion of the Fe^{2+} ions at the surface were converted to Fe^{3+}. The speed at which oxidation occurs is determined by the diffusion speed of the Fe^{2+} ions and by the distance to the surface of the particle. This is why the particles that are bigger remain unaffected by the oxidation phenomena, while the small particles can be oxidized even at room temperature.

At temperature higher than 300 °C, magnetite is oxidized at hematite (α-Fe_2O_3) [10]. This is antiferromagnetic, as a consequence this conversion can damage if is used in specific applications.

The chemistry of the surface and its proprieties are especially important for specific applications. The iron atoms from the surface of the magnetite which are not bound by the oxygen act as Lewis acids, and coordinate the molecules that can donate a pair of electrons. In aqueous systems, these atoms coordinate the water molecules that dissociate quickly resulting in surface functionalized magnetite with hydroxyl groupings like Fe-OH. In this way the chemistry of the magnetite particles is strongly dependent on the pH values; at low pH values the surface of the magnetite particles is charged positively, and at high pH values it is charged negatively (Fig. 7.2). The hydroxyl groupings formed at the surface of the magnetite have an amphoteric character.

7.2.2 Methods for Synthesis of Magnetic Nanoparticles

In the last years numerous research were focused on the synthesis of magnetic nanoparticles. Many scientific publications described efficient methods for synthesis that allows the obtaining of single dispersed magnetic nanoparticles stable in time and with controllable shape.

The synthesis of magnetic nanoparticles experienced substantial progress in the last years but with all of these the high-quality magnetic nanoparticles with controllable proprieties represent a continuous challenge.

The superparamagnetic nanoparticles synthesis is a complex process. First of all an appropriate method of synthesis, that does not involve complicated purification steps and that can be used on industrial scale, must be selected. The most important stage of this process is represented by the establishment of experimental conditions that can assure the obtaining of nanoparticles with proprieties specific for the application domain.

From the iron oxides, magnetite (Fe_3O_4) and maghemite (γ-Fe_2O_3) are the most used in a variety of fields and can be considered superparamagnetic nanoparticles—in certain synthesis conditions.

In Table 7.1, some of the proprieties of the two oxides are presented [10, 12, 13]. Synthetic iron oxides can be obtained by a number of methods, such as precipitation of iron salts [14–22], thermic decomposing of the organometallic precursors [23–28], sol-gel method [29–32], microemulsion [33–36] laser pyrolysis [37–40], combustion method [41–46], hydrothermal method [47–52], sonochemical method [53–56], etc.; from all these methods the most common and used is Fe^{2+} and Fe^{3+} salts precipitation method.

7.2.2.1 Iron Salts Precipitation Method

The iron salts precipitation method is the most simple and efficient method for obtaining magnetic particles, due to the large quantity of particles that can be synthetized.

This method consists of mixing two salts Fe^{3+} and Fe^{2+} in 2:1 molar ratio, in aqueous media, followed by precipitation of these salts using a precipitation agent (a base) [57]. The chemical reaction equation for the formation of magnetite can be described as follows:

$$Fe^{2+} + 2Fe^{3+} + 8OH^- \rightarrow Fe_3O_4 + 4H_2O \tag{7.1}$$

Table 7.1 Magnetite and maghemite physical and magnetic characteristics

Characteristics	Magnetite	Maghemite
Chemical formula	Fe_3O_4	γ-Fe_2O_3
Color	Black	Brown-red
Density (g/cm^3)	5.18	4.87
Melting temperature (°C)	1,583–1,597	–
Dourness	5.5	5
Magnetism type	Ferromagnetic	Ferromagnetic
Curie temperature (K)	858	820–986
Saturation magnetization (emu/g)	92–100	60–80
Crystallization system	Cubic	Cubic or tetragonal
Structural type	Inverse spinel	Spinel with flows
Network parameter (nm)	$a = 0.8396$	$a = 0.83474$ (cubic)
		$a = 0.8347$, $c = 2.501$ (tetragonal)

The complete precipitation of the magnetite should be produced at pH values from 8 to 14, in a non-oxidative media, since magnetite is sensitive to oxidation resulting in maghemite according to the following reaction:

$$2Fe_3O_4 + \tfrac{1}{2}O_2 \rightarrow 3\gamma Fe_2O_3 \tag{7.2}$$

The precipitation process consists of two steps [10, 11, 58–61]:

- Nucleation, when the species concentration reaches supersaturation;
- Slow increase of the nucleus.

7.2.2.2 Sol-Gel Method

This method consists of hydrolysis and condensation of some precursors in solution that results in obtaining a sol of nanometric particles. Organic condensation leads to the formation of a tridimensional network of metal oxides, called wet gel. Since this reaction occurs at room temperature, thermic treatments are required in order to obtain the final crystalline structure [62, 63].

Gamarra et al. [64] precipitated iron oxyhydroxide (FeOOH) in water in the presence of a surfactant, after which they reduced the Fe^{3+} at Fe^{2+} partially, by a light drying in N_2 atmosphere, obtaining at the end magnetite particles.

This method has certain advantages like [65]:

- Depending on experimental conditions materials with pre-established structure can be obtained;
- The possibility of obtaining some amorphous pure phases and the possibility of obtaining single dispersed particles with a good dimension control;
- The possibility of encapsulating of the iron oxide in different matrices, maintaining the properties and stability of the particles.

7.2.2.3 Microemulsion Method

A microemulsion is an isotopic thermodynamically stable dispersion of two liquids that are immiscible (water and oil), in the presence of surfactant, which forms a film at the interface between oil and water, having the hydrocarbon chain, non-polar, dissolved in oil and the polar group in the aqueous phase [66].

Vidal-Vidal et al. [67] obtained spherical single dispersed maghemite particles covered with oleilamine or oleic acid, which presents a narrow distribution of the dimension between 0.6 and 3.5 nm, with magnetization saturation very high (76.3 Am^2/kg, for uncoated nanoparticles; 35.2 Am^2/kg, for magnetic nanoparticles coated with oleic acid, and 33.2 Am^2/kg for magnetic nanoparticles coated with oleilamine). The results demonstrated that oleilamine acts as a precipitation and bonding agent. Chin and Yaacob [68] demonstrated that by the synthesis of the nanoparticles of iron oxide using microemulsion method, nanoparticles under 10 nm can be obtained.

This method is difficult to control, and the efficiency is low compared with other synthesis methods for magnetic nanoparticles, and the obtained particles are polydispersed.

7.2.2.4 Laser Pyrolysis

Laser pyrolysis from gas phase was demonstrated to be an essential procedure in the synthesis of uniformed iron nanoparticles, where the reactants are diluted, which results in the obtaining of fine particles with narrow distributions for the dimension of the particles and the controlled purity, without congesting them [38, 39].

The method for obtaining the magnetic particles by laser pyrolysis was initiated by Haggerty in 1981 for preparing ultrafine silicon powder [69].

The nanoparticles obtained by laser pyrolysis presents a core-shell structure of Fe/FeO, in which the thickness of the shell is not dependent on initial conditions.

The mean diameter of the particles depends on the laser power and it varies between 4 and 11 nm. In the case of FeO particles with the diameter between 9 and 11 nm, the saturation magnetization of the nanopowder reaches 80 Am^2/kg [70].

Core-shell nanoparticles covered with carbon layer present a special interest for biomedical utilization.

The laser pyrolysis synthesis method is one of the most promising with respect to the industrial scale production of nanopowders with the diameter between 5 and 20 nm.

7.2.2.5 Combustion Method

Combustion method involves a strong exothermal redox reaction, between an oxidant agent and diverse organic reducing agents. Initiation of combustion process

develops through rapid heating of the mixture, at relatively decreased temperature, below 500 °C.

Compared to other methods, combustion method has certain advantages, such as: is a simple method, short reaction time, low energy consumption, and friendly with the environment. Moreover, the end product is directly obtained as a result of combustion, without further calcination, so that without supplementary energy consumption.

Increased interest for this unconventional synthesis method is due to diverse range of variables, through which the combustion processes can be conducted and directed so that the reaction products can be fitted within large limits.

Factors influencing self-propagated combustion reaction are [71, 72]:

- Nature of oxidant agent and combustion agent;
- Molar ratio between combustion agent/oxidant;
- Presence of additives with auxiliary roles;
- Initiation temperature and heating velocity;
- Volume of raw matter mixtures;
- Water amount (water) from raw matters;
- Pressure.

Mukasyan et al. [73] showed that maximum temperature reached during the reaction and reaction duration are two main elements controlling the properties of the resulting powder, mainly the amorphous or crystalline characteristics and size of particles from the reaction product. The difference between particles size obtained by using different combustion agents is explained by different combustion gases amount which is released by different exothermal reactions, and different temperature from the reactant system [74].

Li et al. [75] showed that for different metallic cations, organic combustion agents with different functional groups have different complexion power. This will influence both formation and morphology of the desired product.

McKittrick [71] and Jung [76] declare that utilization of larger amount of combustion agent will result in increased combustion temperature developed during the reaction.

Reduced size of particles is due to increased gases volume, which will induce sample expansion, thus impairing development of particles synthesis and growing in size. Considering this aspect, Ozuna et al. [77] formulated the hypothesis that higher the pressure in raw matter is, higher will be the specific surface of the resulting powder, because the oxidation process is strongly exothermal, and the reaction time is very reduced (~1 s); pressure within the system increases even more, and the resulting combustion gases disintegrate the structure of solid material, thus contributing to significant reduction of particle size and spectacular increase of specific surface.

7.2.2.6 Hydrothermal Method

Hydrothermal method includes diverse wet-chemical technologies for crystallization of substances mixture in a close system (autoclave). Hydrothermal method is successfully used when an increase of iron oxide nanoparticle crystals is desired.

Synthesis of iron oxide magnetic nanoparticles requires high temperatures (above 200 °C) and high pressures (0.3–4 MPa), using two main routs: hydrolysis and oxidation or neutralization of metallic hydroxides mixture. The most important parameters of the process are the solvent, temperature, and reaction time [78].

Chen and Xu [78] demonstrated that the size of Fe_3O_4 particles are increasing as the reaction time increases.

Zheng et al. [79] obtained Fe_3O_4 particles using the hydrothermal method, with particle size of 27 nm, using sodium bis(2-ethylhexyl)sulfosuccinate as surfactant. The magnetite nanoparticles obtained are endowed with superparamagnetic behavior at room temperature.

Wang et al. [80] present obtaining of Fe_3O_4 nanoparticles with high crystalline feature. The nanoparticles size obtained using this method at 140 °C for 6 h was 40 nm, saturation magnetization was 85.8 emu/g, hardly decreased compared to bulk Fe_3O_4 bulk (92 emu/g).

Daou et al. [81] reported obtaining monodispersed magnetite nanoparticles of 39 nm in size, synthesized first by co-precipitation method at 70 °C, followed by a second synthesis phase—hydrothermal treatments at 250 °C. Magnetite nanoparticles obtained by co-precipitation method were 12 nm in size, being oxidized in contact with air.

7.2.2.7 Sonochemical Method

Sonochemical method was largely used in generation of new materials with unusual properties. Chemical effects of ultrasounds seem to be acoustic cavitation, which means that the bubbles are forming, grow, and are implosively falling into fluid, which generates a localized hot spot, as gaseous phase. This method was applied in synthesis of nanocomposites, and its versatility was demonstrated in case of preparing the iron oxide nanoparticles [55]. Vijayakumar et al. [82] reported obtaining of magnetite nanoparticles using the sonochemical method by sonication of iron acetate in water, in absence of air. Particles obtained by this method were 10 nm in size, presenting superparamagnetic behavior and very low saturation magnetization at room temperature (below 1.25 emu/g).

Pinkas et al. [83] obtained amorphous iron oxide with very large specific surface using sonochemical method. They sonicated $Fe(acac)_3$ in small amount of water, in argon atmosphere. Organic content and specific surface of Fe_2O_3 can be controlled by water amount within the reaction mixture. Thus, nanoparticles of 48 m^2/g specific surfaces were obtained for using a solvent and 260 m^2/g when working within humid argon atmosphere.

7.2.3 Stabilization/Functioning of Magnetic Nanoparticles

Although within iron oxide magnetic nanoparticles synthesis there are significant advances, maintenance of their stability over a longer time period, without their agglomeration or precipitation, is a very important issue. Iron oxide magnetic nanoparticles stability is required for almost any application, so that development of effective strategies related to improvement of chemical stability is mandatory.

Agglomeration of magnetic nanoparticles is related to van der Waal's and magnetic forces. Van der Waal's interaction occurs due to fluctuations of electron orbitals from one particle, which induces oscillatory dipoles in a neighbor particle. The simplest and direct method seems to be coating of Fe_3O_4 magnetic nanoparticles with an impenetrable cover, so that the oxygen cannot reach the surface of magnetic particle.

Coating strategies applied to magnetic nanoparticles can be divided into two main groups:

- Cover of magnetic nanoparticles with organic compounds, including surfactants [84–87] and polymers [88–91];
- Coating of magnetic nanoparticles with inorganic compounds, including silica gel [92–94], carbon [95, 96], and precious metals (Au [97, 98], Ag [99]).

Surfactants should have functional chemical moieties capable of interacting with hydroxyl groups on the surface of preformed magnetite particles (hydrogen or covalent bonds) and should be stable within media imposed by application fields.

In case of ferrofluids, the main factors providing their stability are: shape, particle size, and chemical structure of the coating layer, responsible of compatibility with dispersion environment. There are three methods for impairing the contact between magnetic nanoparticles and reduction of dipole–dipole interaction: steric stabilization, electrostatic stabilization, and mix stabilization [100].

Generally, surfactants or polymers can be chemically anchored of physically adsorbed on the surface of magnetic nanoparticles, in single layer or double layer, thus creating repulsive forces in order to balance the van der Waal's and magnetic forces which are acting on the surface of magnetic nanoparticles.

Most usual functional groups which can bind on the surface of magnetite are phosphates, sulfates, and carboxylates [10]. Carboxyl group of oleic acid ($CH_3(CH_2)_7CH{=}CH(CH_2)_7COOH$) is involved in formation of hydrogen bonds with hydroxyl groups from the surface of magnetite particles, and thus the coating of particles and their stabilization against agglomeration. Magnetite particles covered with oleic acid are used for obtaining of magnetic fluids based on hydrocarbons [101, 102].

Willis et al. [103] showed that degradation of oleic acid during thermal decomposition, method used for obtaining iron oxide nano-crystallite, will result in formation of high-quality γ-Fe_2O_3 nano-crystals.

Fauconnier et al. [104] investigated adsorption of citric and gluconic acid on surface of maghemite particles for further use in biomedical application.

Polyethylene glycol (PEG) is a hydrophilic polymer, water-soluble, biocompatible, which can be used in synthesis of biocompatible nanoparticles with increased resistance within blood circulation [105].

Another alternative for magnetite particles coating is represented by use of co-polymers, which conduct to particles core-shell, which possible applications in drug transport and delivery (drug vector).

Kumagai et al. [106] developed a simple method for nanoparticles synthesis, followed by their treatment with copolymer block polyethylene glycole-polyaspartic acid. The nanoparticles obtained by this method are endowed with increased stability and solubility in aqueous solutions and biological media.

Koneracka et al. [107] synthesized double-layer coated magnetite nanoparticles for further dispersion in water. Primary surfactant was sodium oleate ($C_{17}H_{33}COONa$), while secondary surfactant was polyethylene glycol which is a biocompatible surfactant. Magnetic nanofluid is used in generation of polymeric nanospheres containing cytostatic drugs.

Moeser et al. [108] prepared magnetite nanoparticles covered with a bifunctional polymer composed of polypropylene oxide, as primary surfactant, and polyacrylic acid anchored with polyethylene oxide chains, as secondary surfactant. Nanoparticles obtained by this method were used in separation of organic compounds from aqueous media.

Utilization of inorganic compounds, such as gold, silver, silica gel, carbon, as surfactants, not only that provides a good stability of the particles, but also allows functionalization of their surface due to engraftment of certain biological ligands.

Silica gel is the most used compound for preparation of iron oxide nanoparticles with functionalized surface, because has few advantages: excellent biocompatibility, hydrophilic ability, integration of other functional groups on its surface, stabilization of iron oxide magnetic nanoparticles in solutions, prevents interactions between particles and their agglomeration, thus providing a better encapsulation [109, 110].

The most common method for synthesis in obtaining magnetic nanoparticles covered with silica is Stöber method [111].

Generally, silica layer increases particle size, so that magnetic properties will be changed. However, the thickness of silica layer can be adjusted by changing TEOS: water ratio, ammonium concentration, hydrolysis time [111].

Many studies described the role of functional groups, which control reactivity and colloidal properties of magnetic suspension, as well as the influence of alkaline reagents, concentration of coated nanoparticles, water/alcohol ratio, or concentration of TEOS on final morphological aspect of these nanostructures [92, 93, 112, 113].

Magnetic nanoparticles using gold as surfactant seem to be ideal, due to its decreased reactivity; however, direct coating of magnetic nanoparticles with gold is very difficult, due to different characteristics of the two surfaces [114–116].

Good coating with carbon layers provides an effective barrier against oxidation and acid erosion of magnetic nanoparticles. So that, it is possible to synthesize magnetic nanoparticles covered with carbon, which are stable from the thermal and

biocompatibility point of view, and which are presenting an increased stability against oxidation, which is crucial for certain application fields [117].

7.2.4 Applications of Magnetic Nanoparticles

Increased interest for magnetic nanoparticles can be explained due to diverse applications of these compounds. The fields in which these particles are used are: biomedical, catalysis, and industrial field. Magnetite particles (Fe_3O_4) dispersed in a fluid were largely used as ferrofluids [118, 119] in diverse applications, such as: electric transformers, pressure transducers, inertial sensors (acceleration, slope, gravity) [120], position sensors [121], devices for information storage [122], heat transfer [123], optics [124, 125], electronics [126], and biomedical engineering [22, 127–130].

7.2.4.1 Applications in Biomedical Field

In case of biomedical applications, colloidal suspensions, obtained because of magnetic nanoparticles dispersion in biological media, should have colloidal stability over a long period. The magnetic core of the particle should respond to an external magnetic field, so that it could be directed and positioned in a certain location, thus facilitating Magnetic Resonance Imaging (MRI) for medical diagnosis, as well as antitumor therapies assisted by alternative magnetic field.

Magnetite and/or maghemite nanoparticles are the most desired for biomedical applications due to their strong ferromagnetic behavior, relatively decreased toxicity, decreased sensitivity to oxidation, as well as increased values of saturation magnetization, compared to other materials (cobalt, nickel, more susceptible to oxidation, with increased toxicity).

Regarding the use of nanoparticles in medical applications, these can be grouped in two main categories: in vivo and in vitro applications. In vivo applications are especially based on diagnostic procedures (MRI) and therapeutic applications (hyperthermia, targeted drug delivery).

Main utilization of magnetic nanoparticles for in vitro experiments is related to diagnosis (cellular separation and selection [131–134], and magnetic relaxometry [135, 136]).

Magnetic resonance imaging (MRI) is a non-invasive technique, without exposure to radiations, which can give transversal imaging within solid material and living organisms [137, 138]. Development of MRI as clinical diagnostic tool largely contributed to pharmaceutical products advance, generating so-called magneto-pharmaceutical products. The purpose of these magneto-pharmaceutical products, in case of clinical use, is to increase the contrast between damaged and healthy tissue, and/or to indicate the function of an organ or blood vessels [139].

These magneto-pharmaceutical products were introduced for the first time as contrast agents, used in magnetic resonance imaging, for localization and diagnostic of brain injuries, myocardial infarction or liver lesions/tumors, where the magnetic nanoparticles have a tendency to highly accumulate, due to differences between tissue composition and endocytotoxic cellular processes [140–143].

Hyperthermia is a therapeutically procedure used for increasing body temperature in a certain region (between 41 and 46 °C, especially in cancer therapy) [144–149]. This technique can be used together with other antitumor treatments (chemotherapy, radiotherapy, and immunotherapy).

Increasing the temperature required for hyperthermia can be accomplished using fine iron oxide magnetic particles. Using an external magnetic field, these particles can be transported and can target the tumor cells. The advantage of hyperthermia is that induces heating of localized magnetic particles and the surrounding tissue, which is enough for destroying the tumor cells, more sensitive to temperature variations.

The first attempt for targeted drug therapy on humans was reported by Lübbe et al. [150], when they used magnetic nanoparticles coated with epirubicin [151] for treatment of solid tumor. Treatment procedure consisted of intravenous infusion of this mixture (magnetic nanoparticles coated with drug) followed by one cycle of chemotherapy. During perfusion and 45 min after, a magnetic field was constructed as close as possible to the tumor site, and they demonstrated that epirubicin-carrying magnetic nanoparticles were successfully directed and transported toward the tumor area.

Effectiveness of this therapy is dependent upon the intensity of magnetic field and the properties of magnetic nanoparticles which are used. Dependent on administration route of drug-carrying magnetic nanoparticles (intravenous, intra-arterial), a series of important parameters should be considered: blood flow, infusion pathway, circulation time, distance from the magnetic source, strength of bound between magnetic nanoparticle-drug, tumor volume, etc. [128, 152].

7.3 Experimental Data

7.3.1 Introduction

In recent years, the design and synthesis of colloidal magnetic suspensions have attracted an increased interest especially in the fields of biotechnology and biomedicine because they have many applications including targeted drug delivery, cell labeling and magnetic cell separation, hyperthermia, tissue repairing, magnetic resonance imaging (MRI) contrast enhancement, enzyme immobilization, immunoassays, protein purification, etc.

Magnetic nanoparticles (MNPs) used in biomedicine must meet several requirements. They have to be non-toxic, chemically stabile, uniform in size, well

stabilized under physiological conditions, biocompatible and to present high magnetization. Magnetite (Fe_3O_4) and maghemite (γ-Fe_2O_3) are the most suitable iron oxide nanoparticles employed for biomedical applications because they are biocompatible, have low toxicity in the human body and show a superparamagnetic behavior.

Therefore, synthesis of magnetic iron oxide nanoparticles with tailored properties has attracted considerable scientific and technological interest. Various synthesis routes were developed for producing magnetic particles, such as co-precipitation, microemulsion method, thermal decomposition of different organic precursors, spray pyrolysis, and sol-gel method.

In the recent years, combustion synthesis has been often reported as a useful method for the preparation of metal oxide nanopowders. Still, there are very few papers dealing with combustion synthesis of Fe_3O_4 nanopowders and virtually there are no studies on the in vitro toxicity of the as-prepared iron oxide nanoparticles. In 2012, Ianoş et al. [46] reported a simple combustion technique for the preparation of Fe_3O_4 nanopowders, which is based on conducting the combustion reaction inside a round bottom flask and evolving gases are bubbled in a beaker filled with water.

For biomedical applications, magnetic iron oxide nanoparticles must be dispersed in biocompatible media in order to obtain stable colloidal suspensions. In order to prevent the particle aggregation and to improve the biocompatibility and stability, nanoparticles are coated with various surfactants: poly(ethylene glycol), oleic acid, poly(acrylic acid), gluconic acid, other polymers, liposome and fatty acids.

In this study, we investigated the influence of colloidal suspensions of magnetic iron oxide nanoparticles on tumor (breast cancer cell line SK-BR-3) and normal (adult bone marrow-derived mesenchymal stem cells (MSCs)) cell lines cultivated in vitro conditions. The MNPs used for the preparation of colloidal suspensions were synthesized using a new version of the combustion method.

As far as we know, this could be the first evaluation of the toxic effects of combustion synthesized magnetic iron oxide nanoparticles. For comparison, magnetite nanoparticles were also prepared by the well-known co-precipitation route. The influence of different concentrations on MNPs on cellular morphology, ultrastructure expression of phenotypical markers, and viability were examined in order to establish whether the combustion synthesized nanoparticles may be used for in vitro and in vivo applications.

7.3.2 Results and Discussion

7.3.2.1 Characterization of Fe_3O_4 Nanoparticles

The main characteristics of iron oxide nanopowders prepared by combustion synthesis (powder 1) and co-precipitation (powder 2) are shown in Table 7.2.

Table 7.2 Characteristics of Fe_3O_4 nanoparticles prepared by solution combustion synthesis [25] (powder 1) and co-precipitation (powder 2), respectively

Powder no.	XRD phase composition	D_{XRD} (nm)	S_{BET} (m^2/g)	D_{TEM} (nm)	M_s (emu/g)	M_r (emu/g)	H_c (kA/m)
1	Fe_3O_4	10	106	15–20	55.3	3.3	3.0
2	Fe_3O_4	9	98	10–15	61.3	0.8	0.5

D_{XRD} crystallite size, S_{BET} specific surface area, D_{TEM} particle size from TEM, M_s saturation magnetization, M_r remanent magnetization, H_c coercivity

One can easily notice that that the two powders are very similar in terms of phase composition (single-phase Fe_3O_4), crystallite size, and specific surface area and particle size.

Considering the magnetic properties of the resulted powders one may notice that the saturation magnetization of the sample prepared by combustion synthesis is slightly smaller than the sample prepared by co-precipitation (Table 7.2). At the same time, the remnant magnetization and the coercivity of combustion synthesized Fe_3O_4 are a little bit larger than the co-precipitated Fe_3O_4, yet very close to the superparamagnetic behavior.

7.3.2.2 Structural Characteristics of Colloidal Suspensions Based on Fe_3O_4 Nanoparticles

After coating the nanoparticles with a double layer of oleic acid, the stabilized nanoparticles were dispersed in phosphate buffer saline (PBS), leading to two sets of stable colloidal fluids, termed 1F (deriving from powder 1) and 2F (deriving from powder 2). TEM analysis conducted on samples 1F and 2F, evidenced that the actual size of combustion synthesized Fe_3O_4 nanoparticles is around 15–20 nm (Fig. 7.3), whilst the co-precipitated magnetite particles have 10–15 nm. Both types of nanoparticles have a sphere-like shape.

The intensity distribution of particle size revealed that the colloidal suspension deriving from combustion synthesized magnetite (sample 1F) has virtually a single family of particles and an average hydrodynamic diameter of 107 nm (Fig. 7.2). On the other hand, the colloidal suspension deriving from the co-precipitated magnetite (sample 2F) has a bimodal particle size distribution, which suggests the presence of two populations of particles (Fig. 7.4).

The average hydrodynamic diameter of sample 2F (61 nm) is smaller when compared to sample 1F. However, in both cases, the hydrodynamic diameter is larger than the core size of Fe_3O_4 nanoparticles observed in TEM images (Fig. 7.3), which is probably due to the presence of oleic acid double layer as well as the possible aggregate formation.

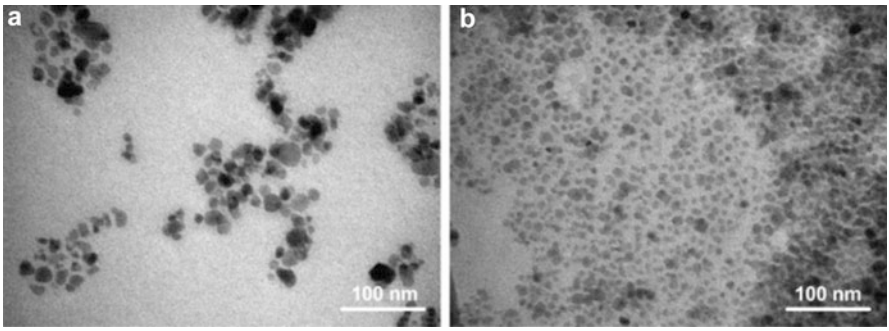

Fig. 7.3 TEM images of colloidal suspensions 1F (**a**) and 2F (**b**)

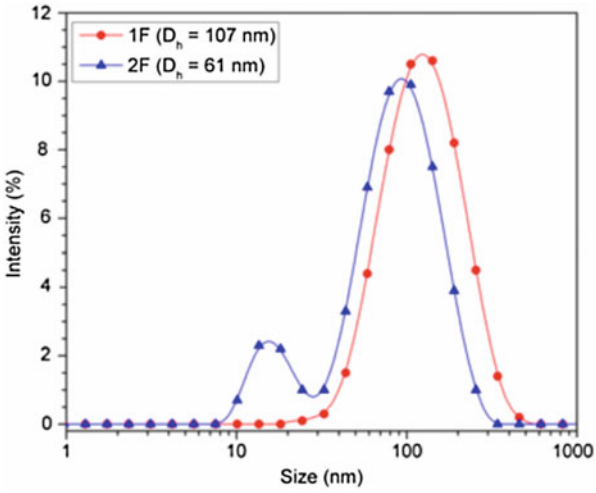

Fig. 7.4 The intensity distribution of particle size (DLS) of suspensions 1F and 2F

7.3.2.3 Ultrastructural and Morphological Cell Changes Induced by Fe_3O_4-Based Colloids

Optic microscopy did not reveal any morphological changes of adult bone marrow-derived mesenchymal stem cells (MSCs) but scanning electron microscopy showed several changes in cellular morphology, of both normal (MSCs) and tumor cells (breast cancer cell line SK-BR-3).

Bone marrow-derived mesenchymal stem cells (MSCs) are fibroblast-like, presenting thin (filopodia) and thick (lamellipodia) elongations for inter-cellular contact and adhesion to substrate (Fig. 7.5a). When fluid 1F was added in culture media for 48 h, MSCs developed cellular protrusions—microtentacles, which is usually associated with increased adhesion capacity (Fig. 7.5b). When fluid 2F was added in culture, MSCs seem to lose their filopodia, become flattened and irregular

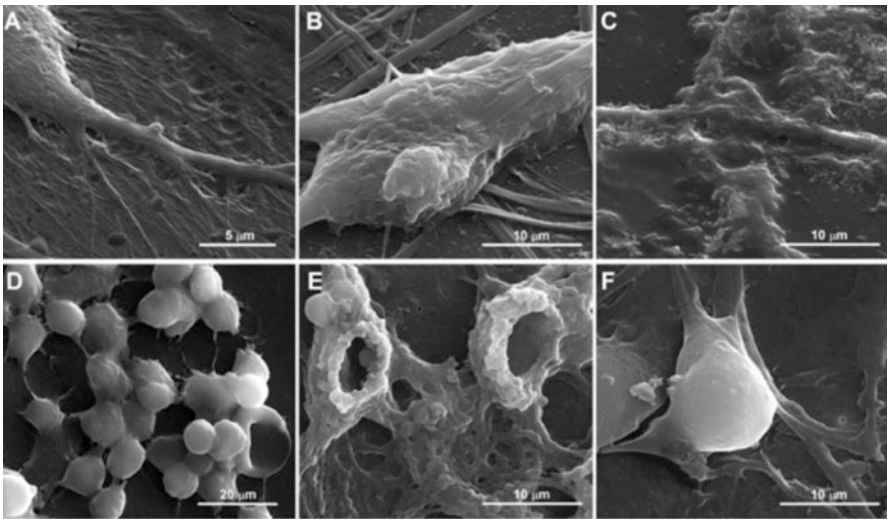

Fig. 7.5 SEM images of MSCs and SK-BR-3 cells before and after the treatment with colloidal suspensions: (**a**) control (untreated) MSCs, (**b**) MSCs treated with suspension 1F, (**c**) MSCs treated with suspension 2F, (**d**) control (untreated) SK-BR-3 cells, (**e**) SK-BR-3 cells treated with suspension 1F, (**f**) SK-BR-3 cells treated with suspension 2F

in morphological appearance, while the magnetite nanoparticles are revealed covering the cell surface (Fig. 7.5c).

Morphological characteristics of SK-BR-3 cells are depicted in Fig. 7.5d, showing the round shape, small diameter and cluster-like growth of this cellular type in vitro, which are forming more like a network of cellular elongations and contact points, with increased deposition of extracellular matrix within the resulted mesh. SK-BR-3 tumor cells presented a very unusual behavior when left in contact with fluid 1F (deriving from combustion synthesized nanoparticles) for 48 h, extruding the nucleus, so that the cells were enucleated (Fig. 7.5e)—which is a very rare phenomenon.

When fluid 2F (deriving from co-precipitated nanoparticles) was added on these tumor cells, they developed thicker elongations and anchorage structures, long, and less interconnected with the surrounding cells (Fig. 7.5f).

Transmission electron microscopy was performed on both cellular types, adherent on cell culture inserts and suspension cells. Ultrastructural description of MSCs focuses on segmented nucleus, multiple elongations, numerous mitochondria and lysosomes, rare endoplasmic reticulum and intracytoplasmic vacuoles (Fig. 7.6a, b).

SK-BR-3 tumor cells are characterized by large nucleus, multiple lipid vacuoles, well represented endoplasmic reticulum distributed along the entire cytoplasm, polyribosomes and mitochondria, showing intense metabolic processes these cells are involved in (Fig. 7.6c, d). Addition of fluid 2F (deriving from co-precipitated nanoparticles) on SK-BR-3 cells determined some morphological changes, inducing accumulation of MNPs at the cytoplasmic level, in large clusters (Fig. 7.7a, b),

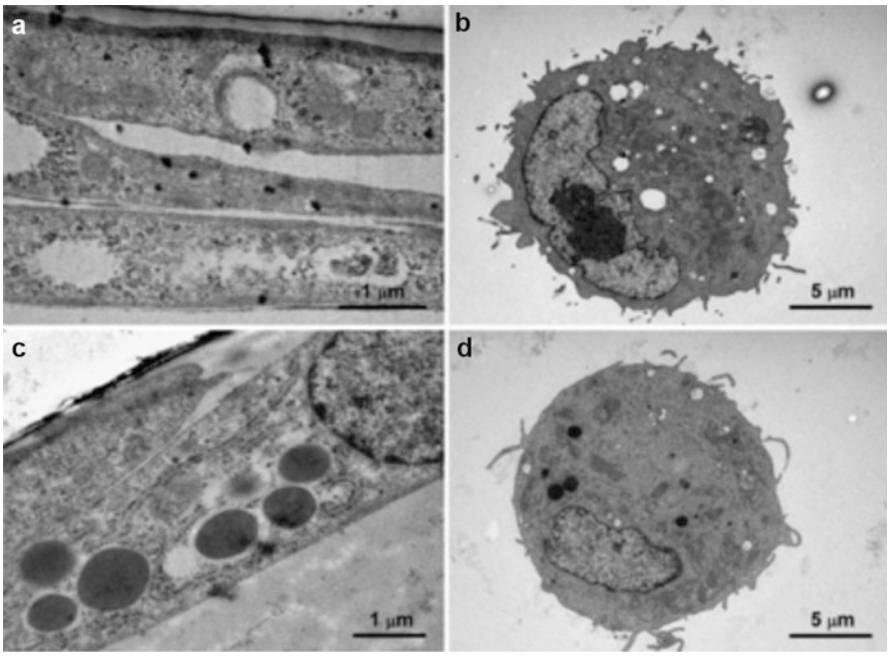

Fig. 7.6 TEM images of untreated control cells: (**a**) adherent MSCs grown in cell culture inserts, (**b**) suspension of MSCs, (**c**) adherent SK-BR-3 cells cultured on cell culture inserts, (**d**) suspension of SK-BR-3 cells

decreased number of mitochondria and occurrence of large vacuoles within the lysosomal structures.

When fluid 1F (deriving from combustion synthesized nanoparticles) was added in culture media, most of the SK-BR-3 (>90 % of the cells, counted on five different TEM images) cells appeared without nucleus (as seen on the SEM image—Fig. 7.5e) and less of the cytoplasmic structures were evidenced. A spiral-like concentrically oriented pattern was distinguished within the entire cytoplasm, revealing the stress fibers inducing the morphological change of cytoskeleton (Fig. 7.7c, d).

Interestingly, the enucleation phenomenon occurred only in the case of SK-BR-3 tumor cells treated with the fluid deriving from combustion synthesized Fe_3O_4 nanoparticles, which might indicate a certain degree of toxic selectivity of these nanoparticles with respect to SK-BR-3 tumor cells. Although the use of superparamagnetic iron oxide nanoparticles (SPIONs) in cancer therapy (hyperthermia) has been widely investigated [1–6, 8, 28–36, 153], no reports were published about the potential use of combustion synthesized Fe_3O_4 nanoparticles in cancer therapy due to their intrinsic selective action on SK-BR-3 tumor cells.

Suspension fixed MSCs treated with the two colloidal suspensions showed the entire inner architecture disturbed, with large lysosomes accumulating the nanoparticles, suggesting an accentuated endocytosis process for removal of iron

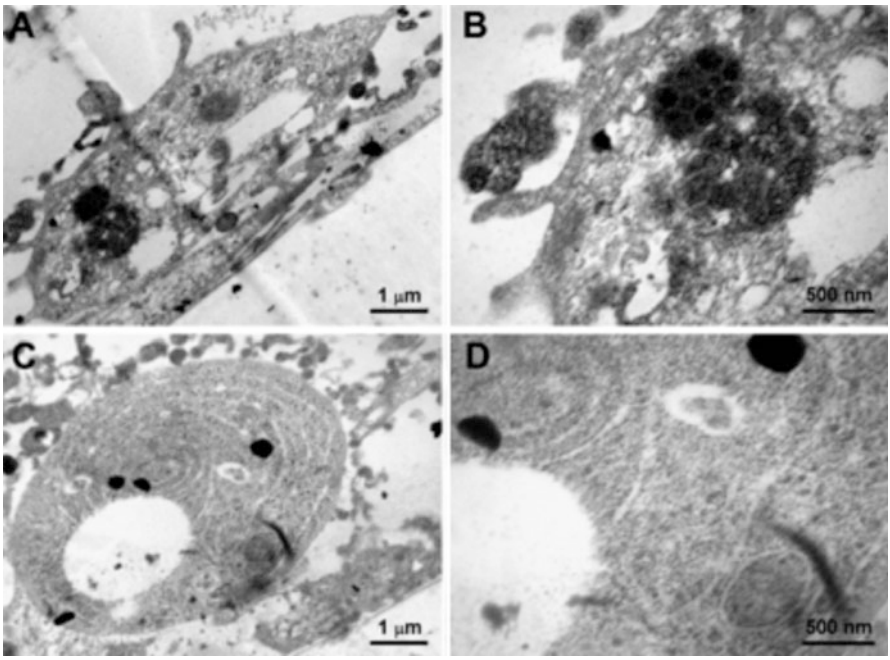

Fig. 7.7 TEM of SK-BR-3 cells treated with colloidal suspensions: (**a**, **b**) SK-BR-3 cells treated with fluid 2F (deriving from co-precipitated nanoparticles), (**c**, **d**) SK-BR-3 cells treated with fluid 1F (deriving from combustion synthesized nanoparticles)

oxide nanoparticles (Fig. 7.8a–d). There is no evidence of stress fibers within the cytoplasm, and the polyribosomes are well represented for both treatments used on these cells (Fig. 7.8a–d).

7.3.2.4 Immunophenotypical Cell Changes Induced by the Addition of Fe_3O_4-Based Colloids

MSCs were stained for cytoskeleton protein vimentin, which does not change the expression pattern within the cytoplasm of MSCs control (Fig. 7.9a), MSCs treated with fluid 1F (Fig. 7.9b) or MSCs treated with fluid 2F (Fig. 7.9c). Morphological analysis shows that MSCs in contact with fluid 1F became more elongated, stretched and fusiform (Fig. 7.9b). SK-BR-3 cells presented initially an increased expression of Her2 oncoprotein (Fig. 7.9d). The expression of this marker was absent/diminished in the case of SK-BR-3 cells treated with suspensions 1F (Fig. 7.9e) and 2F (Fig. 7.9f).

Flowcytometric evaluation of characteristic stem cell markers CD90 and CD73 showed that expression of these molecules on MSCs surface was maintained on cells treated with the suspension 2F deriving from co-precipitated nanoparticles, and decreased significantly on MSCs treated with fluid 1F, prepared from

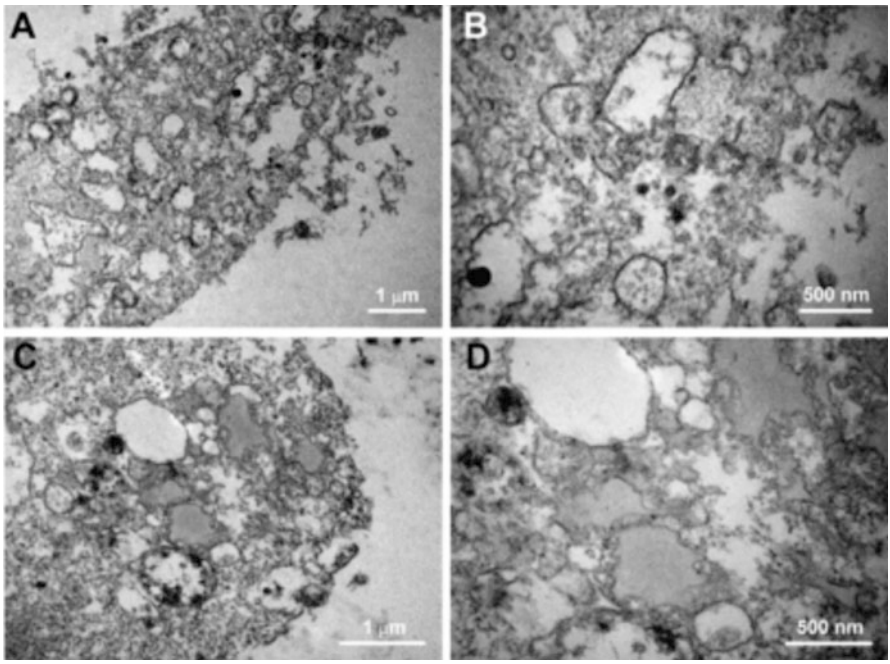

Fig. 7.8 TEM of MSCs treated with colloidal suspensions: (**a**, **b**) MSCs treated with fluid 2F (deriving from co-precipitated nanoparticles), (**c**, **d**) MSCs treated with fluid 1F (deriving from combustion synthesized nanoparticles)

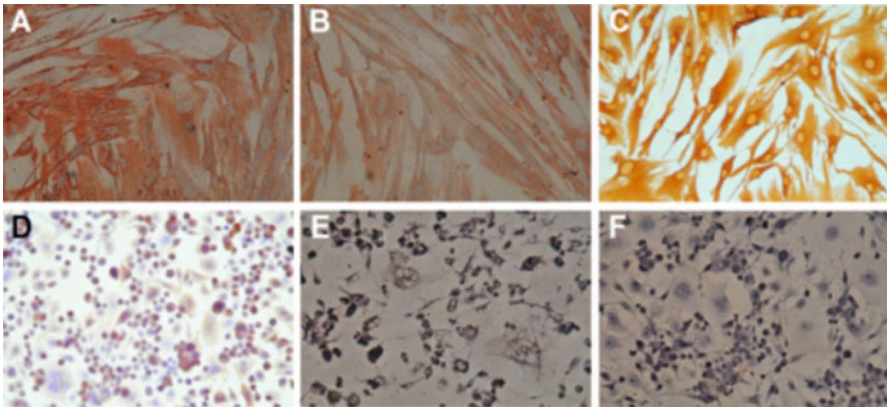

Fig. 7.9 Immunocytochemistry on MSCs and SK-BR3 cells stained for Vimentin and Her2

combustion synthesized nanoparticles. Similar pattern was obtained in case of the other molecule investigated—CD29, which is an adhesion molecule, involved in migratory capacity of these cells (Fig. 7.10).

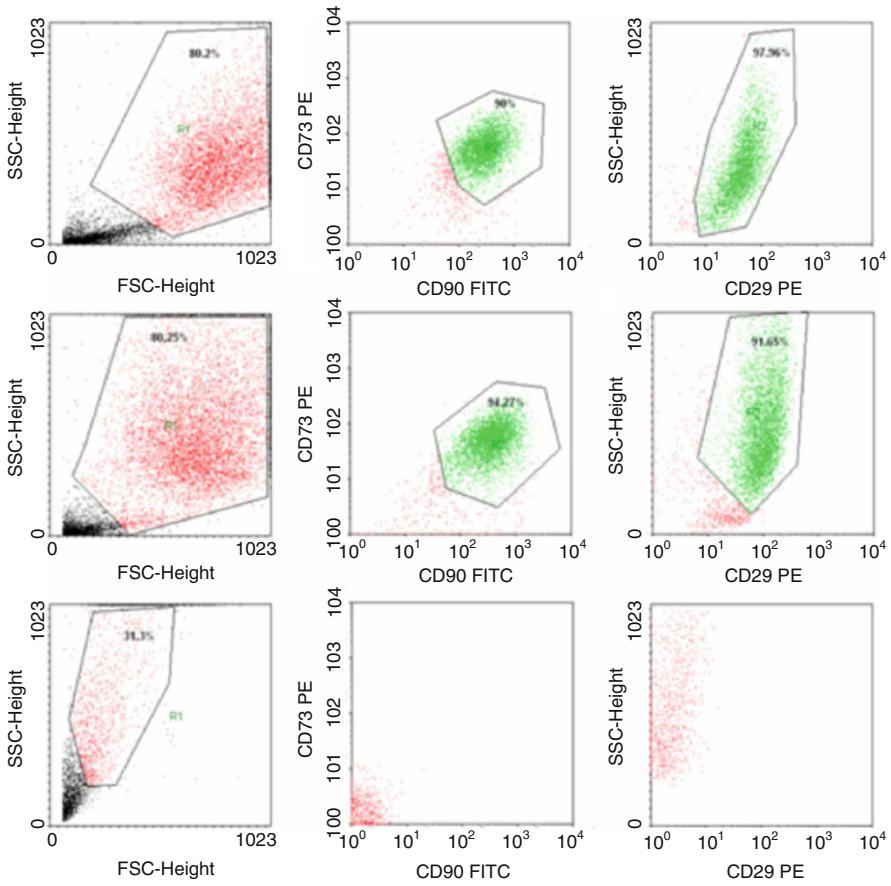

Fig. 7.10 Flowcytometric analysis of MSCs before and after treatment with colloidal suspensions: MSCs control (untreated cells), MSCs treated with fluid 2F, and MSCs treated with fluid 1F

SK-BR-3 tumor cells treated with each of the two colloidal suspensions increased their aggressive potential by highly expressing Her2 oncoprotein on the cellular surface (Fig. 7.11). Another interesting aspect revealed by the flowcytometric analysis is the translation of the SK-BR-3 cells to the left panel of FCS axis and upper part of the SSC axis, suggestive for decreased size and increased granularity of these cells treated with magnetite-based colloids. Data are correlated with TEM images showing accumulation of nanoparticles within the cytoplasm.

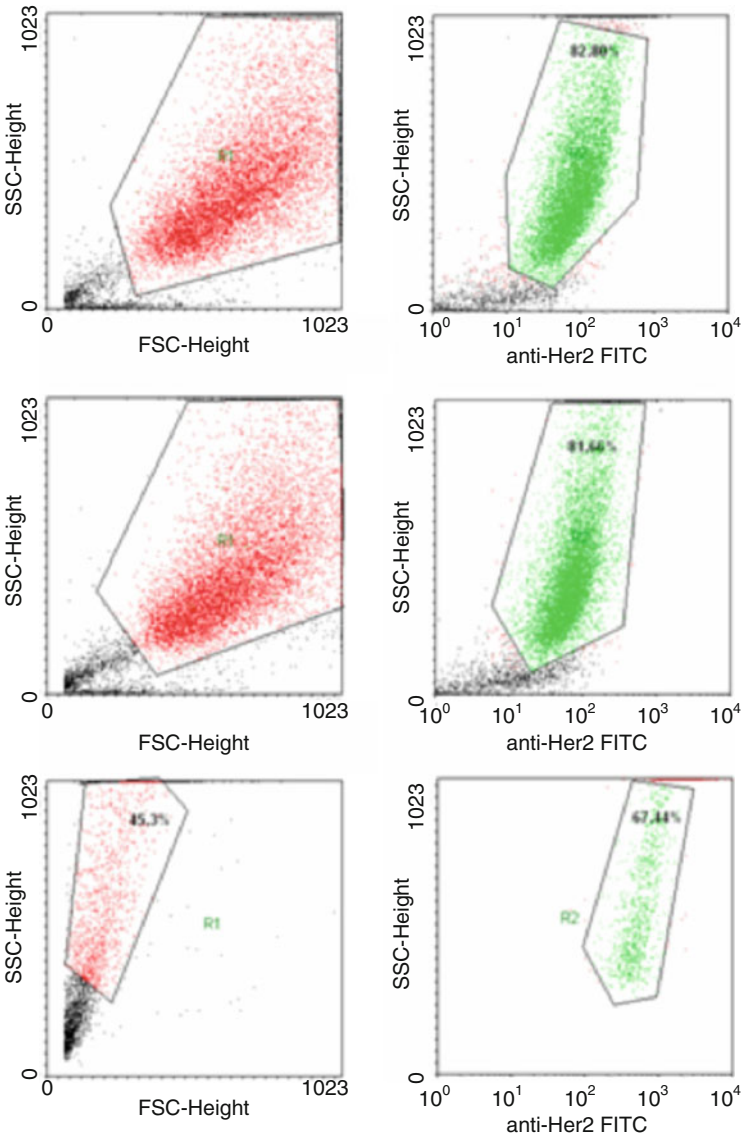

Fig. 7.11 Flowcytometric analysis of SK-BR-3 cells before and after treatment with colloidal suspensions: SK-BR-3 control (untreated cells), SK-BR-3 cells treated with fluid 2F, and SK-BR-3 cells treated with fluid 1F

7.3.2.5 Toxic Effects of Fe_3O_4-Based Colloids

Annexin V-FITC/PI assay was employed to compare the viability of normal MSCs and SK-BR-3 tumor cells after 48 h of co-culture with the two colloidal suspensions

Table 7.3 Results of Annexin V-FITC/PI assay—viability of MSCs and SK-BR-3 tumor cells treated with magnetite-based colloidal suspensions

Cellular type	Substance	Live cells (%)	Apoptotic cells (%)	Dead cells (%)
MSC	Control (untreated)	90.63	7.93	1.44
MSC	Fluid 1F	66.94	7.87	25.20
MSC	Fluid 2F	61.28	30.62	8.10
SK-BR-3	Control (untreated)	73.10	23.35	3.55
SK-BR-3	Fluid 1F	61.87	32.41	5.72
SK-BR-3	Fluid 2F	65.57	27.38	7.05

having a similar concentration of magnetite nanoparticles, $\sim 5 \times 10^{-2}$ mg/mL (Table 7.3).

The viability of MSCs treated with the colloidal suspension deriving from combustion synthesized magnetite (fluid 1F) is higher than that deriving from co-precipitated magnetite (fluid 2F). The viability of SK-BR-3 tumor cells treated with the colloidal suspension deriving from combustion synthesized Fe_3O_4 (fluid 1F) is smaller than that deriving from co-precipitated Fe_3O_4 (fluid 2F).

The results of Annexin V-FITC/PI assay—viability of MSCs and SK-BR-3 tumor cells treated with magnetite-based colloidal suspensions—support the idea that combustion synthesized nanoparticles are more active in reducing the proliferation rate of SK-BR-3 tumor cells. This behavior is in excellent agreement with the enucleation process of SK-BR-3 tumor cells observed on SEM (Fig. 7.5e) and TEM (Fig. 7.7c, d) images.

7.3.3 *Experimental Procedures*

Synthesis of Fe_3O_4 nanoparticles: magnetite nanoparticles were prepared by two different routes, namely solution combustion synthesis and co-precipitation respectively.

(a) Combustion synthesis: an aqueous solution containing $Fe(NO_3)_3 \times 9H_2O$ (Roth, pro analysis) and $C_6H_{12}O_6$ (Riedel de Haën, pro analysis) was heated to 400 °C in the absence of air, in a round bottom flask. As the water evaporates, a smoldering combustion reaction occurs, leading to the formation of a black powder (powder 1) which consists of nanocrystalline Fe_3O_4. A more detailed description of combustion synthesis of magnetite nanoparticles can be found in one of our papers published in 2012 [25]. The resulted black powder was hand crushed, washed with warm distilled water and dried at 80 °C.

(b) Co-precipitation: excess NH_4OH (Chimopar, pro analysis) was added under vigorous stirring to a hot (80 °C) aqueous solution of $FeSO_4 \times 7H_2O$ (Chimopar, pro analysis) and $FeCl_3 \times 6H_2O$ (Merck, pro analysis), according to the procedure reported by Bica [11, 37]. A black precipitate, of single-phase magnetite was obtained (powder 2).

Fe_3O_4 nanoparticle characterization: iron oxide nanoparticles have been characterized in terms of XRD phase composition (Rigaku Ultima IV, $Cu_{K\alpha}$, Tokyo, Japan), specific surface area (nitrogen adsorption–desorption, Micromeritics ASAP 2020 (Micromeritics Instrument Corporation, Norcross, USA)) and magnetic properties (VSM 880 ADE/DMS magnetometer (DMS/ADE Technologies, Massachusetts, USA)).

Preparation of stable colloidal suspensions: Fe_3O_4 nanoparticles prepared by the two synthesis routes have been used to prepare stable colloidal suspensions. For this purpose, the iron oxide nanoparticles prepared by combustion synthesis were sonicated for several hours and then covered with a first layer of oleic acid (Merck, 65–88 %) [11, 37]. In the case of the co-precipitation synthesized particles, the nanoparticles were coated with a first layer of oleic acid as soon as the precipitation reaction started. This step was followed by a washing process with warm fresh distilled water. Subsequently, the pH of the solution containing the magnetic nanoparticles was adjusted to 9 with NH_4OH (Chimopar, pro analysis) and a second layer of oleic acid was achieved by adding some more oleic acid. The oleic acid double layer-coated nanoparticles were dispersed in phosphate buffered saline (PBS—Sigma Aldrich), leading to stable colloidal suspensions termed sample 1F (derived from powder 1, prepared by combustion synthesis) and sample 2F (derived from powder 2, prepared by co-precipitation). The two colloidal suspensions contained a similar amount of Fe_3O_4 nanoparticles (~5×10^{-2} mg/mL).

Colloidal suspension characterization: the resulted colloidal suspensions based on PBS were characterized by dynamic laser scattering (DLS) using a ZetaSizer NanoZS Malvern Instrument (Worcestershire, UK). A drop of diluted aqueous suspension of magnetic nanoparticles (MNPs) was placed on the grids and allowed to air-dry, and transmission electron microscopy (TEM) was performed for diluted MNPs with FEI Tecnai 12 transmission electron microscope (FEI Company, Eindhoven, NL). The in vitro toxicity of colloidal suspensions based on magnetic iron oxide nanoparticles on tumor and normal cell lines was investigated as follows.

Cell lines: unprocessed bone marrow (10 mL) obtained from 10 human adult subjects free of hematological disorders was used for isolation of mesenchymal stem cells (MSCs). Bone marrow-derived human mesenchymal stem cells (MSCs) were isolated following 2 cellular passages based on plastic adherence, fibroblast-like morphology, and were further used in our experiments. The MSCs culture and expansion media contained *alpha*-minimum essential medium (MEM; Gibco BRL, Invitrogen, Carlsbad, CA, USA), supplemented with 10 % fetal calf serum (FCS; PromoCell, Heidelberg, Germany) and 2 % Penicillin/Streptomycin mixture (Pen/Strep, 10,000 IU/mL; PromoCell), and cells were grown at 37 °C in 5 % CO_2 atmosphere. Medium replacement was performed every third days and when reaching 80–90 % confluence, the cells were passed using 0.25 % Trypsin-EDTA solution (Sigma Aldrich Company, Ayrshire, UK) followed by centrifugation (10 min, 300 g) and replated in T75 culture flasks at a density of 10,000 cells/cm^2. SK-BR-3 (breast cancer) cells were procured from American Type Culture Collection (ATCC, Manassas, VA, USA) and further maintained and expanded in McCoy's 5A medium (Gibco) supplemented with 10 % FCS (PromoCell) and 1 %

Pen/Strep solution 10,000 IU/mL (PromoCell) in an incubator, at 37 °C in a humidified and 5 % CO_2 atmosphere. Cells were seeded at 10,000 cells/cm^2 in appropriate well plates and allowed to attach for 24 h previous to MNPs addition. Bone marrow samples were obtained after signing the written informed consent elaborated under an approved protocol by the Ethics Committee of "Victor Babeş" University of Medicine and Pharmacy Timişoara, according to the World Medical Association Declaration of Helsinki.

Cells scanning electron microscopy (*SEM*): scanning electron microscopy was performed for identification of morphological changes in MSCs and SK-BR-3 cell lines induced by the colloidal suspensions. Cells were cultured at 7,000 cells/cm^2 in 24-well format cell culture inserts (BD Labware Europe, Le Pont De Claix, France) and colloidal suspensions were added 48 h after colloidal suspensions addition, cells were pre-fixed for 1 h with 2.5 % buffered glutaraldehyde (in PBS), rinsed three times in PBS, and the 0.4 μm pore-sized membranes were detached from the culture inserts. For better image quality, cells fixed on the membranes were sputter-coated with platinum-palladium and examined with a FEI Quanta 3D FEG electron microscope (FEI Company, Eindhoven, NL) generating digital electron micrographs.

Cells transmission electron microscopy (*TEM*): MSCs and SK-BR-3 tumor cells were employed for investigation of ultrastructural details changes, 72 h after addition of colloidal suspensions in different concentrations. Cells were prefixed for 1 h with glutaraldehyde (2.5 % in PBS), rinsed three times in PBS, and post-fixed for 1 h in osmium acid (2 % in PBS). Dehydration was done in graded acetone in distilled water dilutions, followed by infiltration with Epon resin. Sections of about 100 nm, obtained on a diamond knife (Diatome) with Leica UC6 ultramicrotome were post-stained with lead citrate and uranyl acetate. The grids were examined with a FEI Tecnai 12 transmission electron microscope (FEI Company).

Annexin V/PI assay: because MTT viability assay is based on spectrophotometric detection of color change due to active substrate metabolization in live cells, and the presence of suspended Fe_3O_4 nanoparticles can influence color detection, we used Annexin V-FITC/PI viability assay, which is based on fluorescence emission and is performed on flowcytometer, thus resulting in less ambiguities of results. Annexin V-FITC (Miltenyi Biotec, Gladbach, Germany) was used in cell death flowcytometric studies (apoptosis) combined with Propidium Iodide Staining Solution (BD Biosciences, San Jose, CA, USA) following the manufacturer's protocol. Shortly, 10^6 cells were washed in 1× Annexin V Binding Buffer (BD Pharmigen) and centrifuged at $300 \times g$ for 10 min, resuspended in the same solution and incubated with 10 μL of Annexin V-FITC for 15 min in the dark. After washing the cells with 1 mL specific binding buffer and centrifugation, the cell pellet was resuspended in 500 μL binding buffer and 1 μg/mL of PI solution was added immediately prior to analysis by flowcytometry.

Flowcytometric analysis: MSCs and SK-BR-3 cells in culture 80–90 % confluence were detached using 0.25 % Trypsin-EDTA (Sigma), washed two times with PBS, resuspended in 100 μL PBS at a concentration of 10^5 cells/mL and incubated in the dark at room temperature for 30 min with mouse anti-human

fluorochrome-conjugated antibody at a dilution specified in the manufacturer's protocol. Cells were then washed twice with 1 mL Cell Wash Solution (BD Biosciences, San Jose, CA, USA) each and resuspended in 500 μL of the same solution for further analysis on a four-color capable FACSCalibur (Becton-Dickinson) flow-cytometer. Conjugated antibodies utilized included FITC-conjugated CD90 (BD Pharmingen™), CD44, and Her2 (Abcam), and PE-conjugated CD29 and CD73. Fluorochrome-conjugated antibodies were purchased from BD Pharmingen™ unless otherwise specified. Acquisition and data analyses were performed using CellQuest Pro software (Becton-Dickinson).

Immunocytochemistry/Immunofluorescence: immunohistochemistry was performed for MSCs and SK-BR-3 tumor cell lines. Cells prepared for these analyses were grown in 4-well glass chamber slides, were left to adhere for 24 h, and colloidal suspensions of different concentrations were added. Untreated cells were used as control. 72 h after addition of colloidal suspensions, medium was removed, cells were washed, fixed with 4 % paraformaldehyde and permeabilized with 0.1 % Triton X-100 and then investigated for expression of the proteins of interest, using for labeling the following antibodies: monoclonal mouse anti-swine Vimentin (clone V9), anti-human smooth muscle actin/HRP (clone 1A4), monoclonal anti-human endoglin, CD105 (clone SN6h), and polyclonal rabbit anti-human c-erb-2 oncoprotein, respectively. All primary antibodies were provided by DakoCytomation (Glostrup, Denmark) and tested for human specificity and cross-reactivity. Staining protocol continued with secondary biotinylated antibody binding, substrate addition (EnVision+® System-HRP DAB/AEC for use with primary antibodies; Dako), and hematoxylin counterstaining of the nuclei following the manufacturer's procedures. Microscopy analysis was performed on a Nikon Eclipse E800 microscope.

Conclusions

The influence of stable colloidal suspensions of magnetite nanoparticles (prepared by combustion synthesis as well by co-precipitation route) on tumor (SK-BR-3 breast cancer cell line) and normal (MSCs adult bone marrow-derived mesenchymal stem cells) cell lines cultivated in vitro conditions was investigated. As far as one can tell, this is the first evaluation of the toxic effects of combustion synthesized magnetite nanoparticles.

Experimental results evidenced that combustion synthesized Fe_3O_4 nanoparticles can be used and are compatible to in vitro culture conditions of both normal and tumor cells. After 48 h in culture media, combustion synthesized nanoparticles and co-precipitated nanoparticles decreased the proliferation rate of normal MSCs and SK-BR-3 tumor cells. Viability of normal MSCs treated with combustion synthesized nanoparticles was higher than the viability of MSCs treated with co-precipitated nanoparticles. At the same time, SK-BR-3 tumor cells treated with combustion synthesized

(continued)

nanoparticles had a lower viability when compared to similar cells treated with co-precipitated nanoparticles. Therefore, in terms of cell viability, the combustion synthesized Fe_3O_4 proved to be superior to the co-precipitated magnetite nanoparticles. A very unusual and rare phenomenon was observed in the case of SK-BR-3 tumor cells treated with combustion synthesized nanoparticles, as the SK-BR-3 tumor cells were enucleated and lost their adhesion abilities. On the other hand, in the presence of combustion synthesized nanoparticles normal MSCs developed anchorage structures, which made them more resistant to the chemical stress.

This remarkable behavior of combustion synthesized magnetite nanoparticles opens a whole new perspective on the potential use of combustion synthesized Fe_3O_4 nanoparticles in cancer therapy due to their selective intrinsic behavior, not only due to their superparamagnetic properties (hyperthermia)—as currently reported.

Acknowledgements We would like to thank Alina Tăculescu, PhD; Robert Ianoş, PhD; and Prof. Cornelia Păcurariu, PhD, Politehnica University Timisoara, for their remarkable contribution in characterization and synthesis of MNPs.

References

1. Leslie Pelecky DL, Rieke RD (1996) Magnetic properties of nanostructured materials. Chem Mater 8(8):1770–1783
2. Cullity BD (1972) Introduction to magnetic materials. Addison-Wesley, New-York
3. Hadjipanayis GC, Prinz GA (1991) Science and technology of nanostructured magnetic materials. Plenum Press, New-York
4. Shylesh S, Schünemann V, Thiel WR (2010) Magnetically separable nanocatalysts: bridges between homogeneous and heterogeneous catalysis. Angew Chem Int Ed 49:3428–3459
5. Huber DL (2005) Synthesis, properties, and applications of iron nanoparticles. Small 1 (5):482–501
6. Jun YW, Choi JS, Cheon J (2007) Heterostructured magnetic nanoparticles: their versatility and high performance capabilities. Chem Commun 12:1203–1214
7. Tebble RS, Craik DJ (1969) Magnetic materials. Wiley-Interscience, London
8. West AR (1988) Basic solid state chemistry. Wiley, New York
9. O'Handley RC (2000) Modern magnetic materials—principles and applications. Wiley, New York
10. Cornell RM, Schwertmann U (1996) The iron oxides: structure, properties, reactions, occurrence and uses. VCH, Weinheim, Germany
11. Cornell RM, Schwertmann U (1991) Iron oxides in the laboratory: preparation and characterization. Wiley-VCH Verlag GmbH, Weinheim
12. Jiles D (1998) Introduction to magnetism and magnetic materials, 2nd edn. Chapman & Hall, New York
13. Frankel RB, Moskowitz BM (2003) In: Miller JS, Drillon M (eds) Magnetism: molecules to materials IV: nanosized magnetic materials. Wiley-VCH Verlag GmbH, Weinheim

14. Bee A, Massart R, Neveu S (1995) Synthesis of very fine maghemite particles. J Magn Magn Mater 149(1–2):6–9
15. Kang YS, Risbud S, Rabolt JF, Stroeve P (1996) Synthesis and characterization of nanometer-size Fe_3O_4 and gamma-Fe_2O_3 particles. Chem Mater 8(9):2209–2211
16. Lee JW, Isobe T, Senna M (1996) Magnetic properties of ultrafine magnetite particles and their slurries prepared via in-situ precipitation. Colloids Surf A Physicochem Eng Asp 109:121–127
17. Kim DK, Zhang Y, Voit W, Rao KV, Muhammed M (2001) Synthesis and characterization of surfactant-coated superparamagnetic monodispersed iron oxide nanoparticles. J Magn Magn Mater 225(1–2):30–36
18. Jolivet JP, Chaneac C, Tronc E (2004) Iron oxide chemistry. From molecular clusters to extended solid networks. Chem Commun 5:481–487
19. Si S, Kotal A, Mandal TK, Giri S, Nakamura H, Kohara T (2004) Size-controlled synthesis of magnetite nanoparticles in the presence of polyelectrolytes. Chem Mater 16(18):3489–3496
20. Tartaj P, Morales MP, Gonzalez-Carreno T, Veintemillas-Verdaguer S, Serna CJ (2005) Advances in magnetic nanoparticles for biotechnology applications. J Magn Magn Mater 290:28–34
21. Wu W, He Q, Hu R, Huang J, Chen H (2007) Preparation and characterization of magnetite Fe_3O_4 nanopowders. Rare Metal Mat Eng 36(3):238–243
22. Laurent S, Forge D, Port M, Roch A, Robic C, Vander Elst L, Muller R (2008) Magnetic iron oxide nanoparticles: synthesis, stabilization, vectorization, physicochemical characterizations and biological applications. Chem Rev 108(6):2064–2110
23. Rockenberger J, Scher EC, Alivisatos AP (1999) A new nonhydrolytic single-precursor approach to surfactant-capped nanocrystals of transition metal oxides. J Am Chem Soc 121 (49):11595–11596
24. Hyeon T, Lee SS, Park J, Chung Y, Bin NH (2001) Synthesis of highly crystalline and monodisperse maghemite nanocrystallites without a size-selection process. J Am Chem Soc 123(51):12798–12801
25. Sun SH, Zeng H (2002) Size-controlled synthesis of magnetite nanoparticles. J Am Chem Soc 124(28):8204–8205
26. Hyeon T (2003) Chemical synthesis of magnetic nanoparticles. Chem Commun 8:927–934
27. Sun SH, Zeng H, Robinson DB, Raoux S, Rice PM, Wang SX, Li GX (2004) Monodisperse MFe_2O_4 (M = Fe, Co, Mn) nanoparticles. J Am Chem Soc 126(1):273–279
28. Woo K, Hong J, Choi S, Lee HW, Ahn JP, Kim CS, Lee SW (2004) Easy synthesis and magnetic properties of iron oxide nanoparticles. Chem Mater 16(14):2814–2818
29. Răileanu M, Crişan M, Petrache C, Crişan D, Zaharescu M (2003) Fe_2O_3-SiO_2 nanocomposites obtained by different sol-gel routes. J Optoelectron Adv Mater 5(3):693–698
30. Ismail AA (2005) Synthesis and characterization of Y_2O_3/Fe_2O_3/TiO_2 nanoparticles by sol-gel method. Appl Catal B Environ 58(1–2):115–121
31. Durães L, Costa BFO, Vasques J, Campos J, Portugal A (2005) Phase investigation of as-prepared iron oxide/hydroxide produced by sol-gel synthesis. Mater Lett 59(7):859–863
32. Dai ZF, Meiser F, Mohwald H (2005) Nanoengineering of iron oxide and iron oxide/silica hollow spheres by sequential layering combined with a sol-gel process. J Colloid Interface Sci 288(1):298–300
33. Hirai T, Mizumoto JY, Shiojiri S, Komasawa I (1997) Preparation of Fe oxide and composite Ti-Fe oxide ultrafine particles in reverse micellar systems. J Chem Eng Jpn 30(5):938–943
34. Liu C, Zou BS, Rondinone AJ, Zhang ZJ (2000) Reverse micelle synthesis and characterization of superparamagnetic $MnFe_2O_4$ spinel ferrite nanocrystallites. J Phys Chem B 104 (6):1141–1145
35. Santra S, Tapec R, Theodoropoulou N, Dobson J, Hebard A, Tan WH (2001) Synthesis and characterization of silica-coated iron oxide nanoparticles in microemulsion: the effect of nonionic surfactants. Langmuir 17(10):2900–2906

36. Yang HH, Zhang SQ, Chen XL, Zhuang ZX, Xu JG, Wang XR (2004) Magnetite-containing spherical silica nanoparticles for biocatalysis and bioseparations. Anal Chem 76(5):1316–1321
37. Bi XX, Ganguly B, Huffman GP, Huggins FE, Endo M, Eklund PC (1993) Nanocrystalline α-Fe, Fe_3C, and Fe_7C_3 produced by CO_2-laser pyrolysis. J Mater Res 8(7):1666–1674
38. Hofmeister H, Huisken F, Kohn B, Alexandrescu R, Cojocaru S, Crunteanu A, Morjan I, Diamandescu L (2001) Filamentary iron nanostructures from laser-induced pyrolysis of iron pentacarbonyl and ethylene mixtures. Appl Phys Mater Sci Process 72(1):7–11
39. He YQ, Li XG, Swihart MT (2005) Laser-driven aerosol synthesis of nickel nanoparticles. Chem Mater 17(5):1017–1026
40. Leconte Y, Veintemillas-Verdaguer S, Morales MP, Costo R, Rodriguez I, Bonville P, Bouchet-Fabre B, Herlin-Boime N (2007) Continuous production of water dispersible carbon-iron nanocomposites by laser pyrolysis: application as MRI contrasts. J Colloid Interface Sci 313(2):511–518
41. Varma A, Lebrat JP (1992) Combustion synthesis of advanced materials. Chem Eng Sci 47 (9–11):2179–2194
42. Patil KC, Aruna ST, Ekambaram S (1997) Combustion synthesis. Curr Opin Solid State Mater Sci 2:158–165
43. Mukasyan AS, Epstein P, Dinka P (2007) Solution combustion synthesis of nanomaterials. Proc Combust Inst 31(2):1789–1795
44. Patil KC, Hegdeg MS, Ratan T, Aruna ST (2008) Chemistry of nanocrystalline oxide materials. Combustion synthesis. Properties and applications. World Scientific, Singapore
45. Aruna ST, Mukasyan AS (2008) Combustion synthesis and nanomaterials. Curr Opin Solid State Mater Sci 12(3–4):44–50
46. Ianoş R (2009) An efficient solution for the single step synthesis of $4CaO{\cdot}Al_2O_3{\cdot}Fe_2O_3$ powders. J Mater Res 24(1):245–252
47. Murakami S, Hosono T, Jezadevan B, Kamitakahara M, Iouku K (2008) Hydrothermal synthesis of magnetite/hydroxyapatite composite material for hyperthermia therapy for bone cancer. J Ceram Soc Jpn 116:950–954
48. Giri S, Samanta S, Maji S, Ganguli S, Bhaumik A (2005) Magnetic properties of alpha-Fe_2O_3 nanoparticle synthesized by a new hydrothermal method. J Magn Magn Mater 285(1–2):296–302
49. Mao B, Kang Z, Wang E, Lian S, Gao L, Tian C, Wang C (2006) Synthesis of magnetite octahedrons from iron powders through a mild hydrothermal method. Mater Res Bull 41 (12):2226–2231
50. Liu X, Qiu G, Yan A, Wang Z, Li X (2007) Hydrothermal synthesis and characterization of alpha-FeOOH and alpha-Fe_2O_3 uniform nanocrystallines. J Alloys Compd 433(1–2):216–220
51. Zhu H, Yang D, Zhu L (2007) Hydrothermal growth and characterization of magnetite (Fe_3O_4) thin films. Surf Coating Tech 201(12):5870–5874
52. Yang X, Jiang W, Liu L, Chen B, Wu S, Sun D, Li F (2012) One-step hydrothermal synthesis of highly water-soluble secondary structural Fe_3O_4 nanoparticles. J Magn Magn Mater 324:2249–2257
53. Kim EH, Lee HS, Kwak BK, Kim BK (2005) Synthesis of ferrofluid with magnetic nanoparticles by sonochemical method for MRI contrast agent. J Magn Magn Mater 289:328–330
54. Bang JH, Suslick KS (2007) Sonochemical synthesis of nanosized hollow hematite. J Am Chem Soc 129(8):2242–2243
55. Teo BM, Chen F, Hatton AT, Grieser F, Ashokkumar M (2009) Novel one-pot synthesis of magnetite latex nanoparticles by ultrasound irradiation. Langmuir 25(5):2593–2595
56. Feng J, Mao J, Wen XG, Tu MJ (2011) Ultrasonic-assisted in situ synthesis and characterization of superparamagnetic Fe_3O_4 nanoparticles. J Alloys Compd 509:9093–9097
57. Khalafalla SE, Reimers GW (1973) Magnetofluids and their manufacture, US Patent 3764540

58. Boistelle R, Astier JP (1988) Crystallization mechanisms in solution. J Cryst Growth 90:14–30
59. Gribanov NM, Bibik EE, Buzunov OV, Naumov VN (1990) Physicochemical regularities of obtaining highly dispersed magnetite by the method of chemical condensation. J Magn Magn Mater 85(1–3):7–10
60. Sugimoto T (2003) Formation of monodispersed nano- and micro-particles controlled in size, shape, and internal structure. Chem Eng Tech 26(3):313–321
61. Schwarzer HC, Peukert W (2004) Tailoring particle size through nanoparticle precipitation. Chem Eng Comm 191(4):580–606
62. Liu XQ, Tao SW, Shen YS (1997) Preparation and characterization of nanocrystalline alpha-Fe_2O_3 by a sol-gel process. Sensor Actuator B Chem 40(2–3):161–165
63. Kojima K, Miyazaki M, Mizukami F, Maeda K (1997) Selective formation of spinel iron oxide in thin films by complexing agent-assisted sol-gel processing. J Sol-Gel Sci Technol 8 (1–3):77–81
64. Gamarra LF, Brito GES, Pontuschka WM, Amaro E, Parma AHC, Goya GF (2005) Biocompatible superparamagnetic iron oxide nanoparticles used for contrast agents: a structural and magnetic study. J Magn Magn Mater 289:439–441
65. Răileanu M, Crişan M, Petrache C, Crişan D, Jitianu A, Zaharescu M, Predoi D, Kuncser V, Filoti G (2005) Sol-Gel Fe_xO_y-SiO_2 nanocomposites. Rom J Phy 50(5–6):595–606
66. Bagwe RP, Kanicky JR, Palla BJ, Patanjali PK, Shah DO (2001) Improved drug delivery using microemulsions: rationale, recent progress, and new horizons. Crit Rev Ther Drug Carrier Syst 18(1):77–140
67. Vidal-Vidal J, Rivas J, Lopez-Quintela MA (2006) Synthesis of monodisperse maghemite nanoparticles by the microemulsion method. Colloids Surf A Physicochem Eng Asp 288(1–3):44–51
68. Chin AB, Yaacob II (2007) Synthesis and characterization of magnetic iron oxide nanoparticles via w/o microemulsion and Massart's procedure. J Mater Process Technol 191(1–3):235–237
69. Haggerty JS (1981) Controlling powder size with collimated light beam—which selectively vaporises larger particles. US Patent Number US4289952-A
70. Morjan I, Alexandrescu R, Dumitrache F, Birjega R, Fleacă C, Soare I et al (2010) Iron oxide-based nanoparticles with different mean sizes obtained by the laser pyrolysis: structural and magnetic properties. J Nanosci Nanotechnol 10(2):1223–1234
71. McKittrick J, Shea LE, Bacalski CF, Bosze EJ (1999) The influence of processing parameters on luminescent oxides produced by combustion synthesis. Displays 19(4):169–172
72. Garcia R, Hirata GA, McKittrick J (2001) New combustion synthesis technique for the production of $(In_xGa_{1-x})_2O_3$ powders: hydrazine/metal nitrate method. J Mater Res 16 (4):1059–1065
73. Mukasyan AS, Costello C, Sherlock KP, Lafarga D, Varma A (2001) Perovskite membranes by aqueous combustion synthesis: synthesis and properties. Sep Purif Technol 25(1–3):117–126
74. Luo XX, Cao WH, Xing MM (2006) Preparation of nano Y_2O_2S:Eu phosphor by ethanol assisted combustion synthesis method. J Rare Earths 24(1):20–24
75. Li F, Hu K, Li JL, Zhang D, Chen G (2002) Combustion synthesis of gamma-lithium aluminate by using various fuels. J Nucl Mater 300(1):82–88
76. Jung CH, Park JY, Oh SJ, Park HK, Kim YS, Kim DK, Kim JH (1998) Synthesis of Li_2TiO_3 ceramic breeder powders by the combustion process. J Nucl Mater 253:203–212
77. Ozuna O, Hirata GA, McKittrick J (2004) Pressure influenced combustion synthesis of gamma- and alpha-Al_2O_3 nanocrystalline powders. J Phys Condens Matter 16(15):2585–2591
78. Chen D, Xu R (1998) Hydrothermal synthesis and characterization of nanocrystalline Fe_3O_4 powders. Mater Res Bull 33(7):1015–1021

79. Zheng YH, Cheng Y, Bao F, Wang YS (2006) Synthesis and magnetic properties of Fe_3O_4 nanoparticles. Mater Res Bull 41(3):525–529
80. Wang J, Sun JJ, Sun Q, Chen QW (2003) One-step hydrothermal process to prepare highly crystalline Fe_3O_4 nanoparticles with improved magnetic properties. Mater Res Bull 38 (7):1113–1118
81. Daou TJ, Pourroy G, Begin-Colin S, Greneche JM, Ulhaq-Bouillet C, Legare P, Bernhardt P, Leuvrey C, Rogez G (2006) Hydrothermal synthesis of monodisperse magnetite nanoparticles. Chem Mater 18(18):4399–4404
82. Vijayakumar R, Koltypin Y, Felner I, Gedanken A (2000) Sonochemical synthesis and characterization of pure nanometer-sized Fe_3O_4 particles. Materials Science and Engineering A-Structural Materials Properties Microstructure and Processing 286(1):101–105
83. Pinkas J, Reichlova V, Zboril R, Moravec Z, Bezdicka P, Matejkova J (2008) Sonochemical synthesis of amorphous nanoscopic iron(III) oxide from $Fe(acac)_3$. Ultrason Sonochem 15 (3):257–264
84. Sahoo Y, Pizem H, Fried T, Golodnitsky D, Burstein L, Sukenik CN, Markovich G (2001) Alkyl phosphonate/phosphate coating on magnetite nanoparticles: a comparison with fatty acids. Langmuir 17(25):7907–7911
85. Vékás L, Bica D, Marinică O (2006) Magnetic nanofluids stabilized with various chain length surfactants. Rom Rep Phys 58(3):257–267
86. Jiang W, Wu Y, He B, Zeng X, Lai K, Gu Z (2010) Effect of sodium oleate as a buffer on the synthesis of superparamagnetic magnetite colloids. J Colloid Interface Sci 347:1–7
87. Mourdikoudis S, Liz-Marzán LM (2013) Oleylamine in nanoparticle synthesis. Chem Mater 25:1465–1476
88. Euliss LE, Grancharov SG, O'Brien S, Deming TJ, Stucky GD, Murray CB, Held GA (2003) Cooperative assembly of magnetic nanoparticles and block copolypeptides in aqueous media. Nano Lett 3(11):1489–1493
89. Liu XQ, Guan YP, Ma ZY, Liu ZH (2004) Surface modification and characterization of magnetic polymer nanospheres prepared by miniemulsion polymerization. Langmuir 20 (23):10278–10282
90. Hong R, Fischer NO, Emrick T, Rotello VM (2005) Surface PEGylation and ligand exchange chemistry of FePt nanoparticles for biological applications. Chem Mater 17(18):4617–4621
91. Alsmadi NA, Wadajkar AS, Cui W, Nguyen KT (2011) Effects of surfactants on properties of polymer-coated magnetic nanoparticles for drug delivery application. J Nanopart Res 13 (12):7177–7186
92. de Almeida MPS, Caiado KL, Sartoratto PPC, Cintra e Silva DO, Rereira AR, Morais PC (2010) Preparation and size-modulation of silica-coated maghemite nanoparticles. J Alloy Comp 500:149–152
93. Roca AG, Carmona D, Miguel-Sancho N, Bomati-Miguel O, Balas F, Piquer C, Santamaria J (2012) Surface functionalization for tailoring the aggregation and magnetic behaviour of silica-coated iron oxide nanostructures. Nanotechnology 23(15):155603
94. Singh RK, Kim TH, Patel KD, Knowles JC, Kim HW (2012) Biocompatible magnetite nanoparticles with varying silica-coating layer for use in biomedicine: physicochemical and magnetic properties, and cellular compatibility. J Biomed Mater Res A 100(7):1734–1742
95. Lu AH, Schmidt W, Matoussevitch N, Bönnemann H, Spliethoff B, Tesche B, Bill E, Kiefer W, Schüth F (2004) Nanoengineering of a magnetically separable hydrogenation catalyst. Angew Chem Int Ed 43:4303–4306
96. Luo N, Liu KX, Liu ZY, Li XJ, Chen SY, Shen Y, Chen TW (2012) Controllable synthesis of carbon coated iron-based composite nanoparticles. Nanotechnology 23(47):475603
97. Lin J, Zhou WL, Kumbhar A, Wiemann J, Fang JY, Carpenter EE, O'Connor CJ (2001) Gold-coated iron (Fe@Au) nanoparticles: synthesis, characterization, and magnetic field-induced self-assembly. J Solid State Chem 159(1):26–31

98. Mohammad F, Balaji G, Weber A, Uppu RM, Kumar CSSR (2010) Influence of gold nanoshell on hyperthermia of superparamagnetic iron oxide nanoparticles. J Phys Chem C 114(45):19194–19201
99. Sobal NS, Hilgendorff M, Mohwald H, Giersig M, Spasova M, Radetic T, Farle M (2002) Synthesis and structure of colloidal bimetallic nanocrystals: the non-alloying system Ag/Co. Nano Lett 2(6):621–624
100. Vékás L (2013) Magnetic nanofluids. Synthesis, stabilization, properties, applications. Romanian Academy Publ. House, Bucharest
101. Bica D (1995) Preparation of magnetic fluids for various applications. Rom Rep Phys 47(3–5):265–272
102. Bica D, Vékás L, Avdeev MV, Marinică O, Socoliuc V, Bălăşoiu M, Garamus VM (2007) Sterically stabilized water based magnetic fluids: synthesis, structure and properties. J Magn Magn Mater 311:17–21
103. Willis AL, Turro NJ, O'Brien S (2005) Spectroscopic characterization of the surface of iron oxide nanocrystals. Chem Mater 17(24):5970–5975
104. Fauconnier N, Bee A, Roger J, Pons JN (1996) Adsorption of gluconic and citric acids on maghemite particles in aqueous medium. Progr Colloid Polymer Sci 100:212–216
105. Moghimi SM, Hunter AC, Murray JC (2001) Long-circulating and target-specific nanoparticles: theory to practice. Pharmacol Rev 53(2):283–318
106. Kumagai M, Imai Y, Nakamura T, Yamasaki Y, Sekino M, Ueno S, Hanaoka K, Kikuchi K, Nagano T, Kaneko E, Shimokado K, Kataoka K (2007) Iron hydroxide nanoparticles coated with poly(ethylene glycol)-poly(aspartic acid) block copolymer as novel magnetic resonance contrast agents for in vivo cancer imaging. Colloids Surf B Biointerfaces 56(1–2):174–181
107. Koneracka M, Muckova M, Zavisova V, Tomasovicova N, Kopcansky P, Timko M, Jurikova A, Csach K, Kavecansky V, Lancz G (2008) Encapsulation of anticancer drug and magnetic particles in biodegradable polymer nanospheres. J Phys Condens Matter 20 (20):204151
108. Moeser GD, Green WH, Laibinis PE, Linse P, Hatton TA (2004) Structure of polymer-stabilized magnetic fluids: small-angle neutron scattering and mean-field lattice modeling. Langmuir 20(13):5223–5234
109. Bruce IJ, Taylor J, Todd M, Davies MJ, Borioni E, Sangregorio C, Sen T (2004) Synthesis, characterisation and application of silica-magnetite nanocomposites. J Magn Magn Mater 284:145–160
110. Alcala MD, Real C (2006) Synthesis based on the wet impregnation method and characterization of iron and iron oxide-silica nanocomposites. Solid State Ion 177(9–10):955–960
111. Stöber W, Fink A, Bohn E (1968) Controlled growth of monodisperse silica spheres in the micron size range. J Colloid Interface Sci 26(1):62–69
112. van Blaaderen A, Kentgens APM (1992) Particle morphology and chemical microstructure of colloidal silica spheres made from alkoxysilanes. J Non Cryst Solids 149(3):161–178
113. Wang H, Nakamura H, Yao K, Maeda H, Abe E (2001) Effect of solvents on the preparation of silica-coated magnetic particles. Chem Lett 11:1168–1169
114. Cho SJ, Idrobo JC, Olamit J, Liu K, Browning ND, Kauzlarich SM (2005) Growth mechanisms and oxidation resistance of gold-coated iron nanoparticles. Chem Mater 17(12):3181–3186
115. Wang LY, Luo J, Maye MM, Fan Q, Qiang RD, Engelhard MH, Wang CM, Lin YH, Zhong CJ (2005) Iron oxide-gold core-shell nanoparticles and thin film assembly. J Mater Chem 15 (18):1821–1832
116. Căruntu D, Cushing BL, Căruntu G, O'Connor CJ (2005) Attachment of gold nanograins onto colloidal magnetite nanocrystals. Chem Mater 17(13):3398–3402
117. Chan HBS, Ellis BL, Sharma HL, Frost W, Caps V, Shields RA, Tsang SC (2004) Carbon-encapsulated radioactive Tc-99m nanoparticles. Adv Mater 16(2):144–149
118. Rosensweig RE (1989) Magnetic fluids: phenomena and process applications. Chem Eng Progr 85(4):53–61

119. Raj K, Moskowitz B, Casciari R (1995) Advances in ferrofluid technology. J Magn Magn Mater 149(1–2):174–180
120. Vékás L (2009) Ferrofluids and magnetorheological fluids. Adv Sci Technol 54:127–136
121. Raj K, Moskowitz B (1990) Commercial applications of ferrofluids. J Magn Magn Mater 85 (1–3):233–245
122. Todorovic M, Schultz S, Wong J, Scherer A (1999) Writing and reading of single magnetic domain per bit perpendicular patterned media. Appl Phys Lett 74(17):2516–2518
123. Blums E (1995) Some new problems of complex thermomagnetic and diffusion-driven convection in magnetic colloids. J Magn Magn Mater 149(1–2):111–115
124. Philip J, Rao CB, Jayakumar T, Raj B (2000) A new optical technique for detection of defects in ferromagnetic materials and components. NDT Int 33(5):289–295
125. Philip J, Jaykumar T, Kalyanasundaram P, Raj B (2003) A tunable optical filter. Meas Sci Tech 14(8):1289–1294
126. Chiba D, Yamanouchi M, Matsukura F, Ohno H (2003) Electrical manipulation of magnetization reversal in a ferromagnetic semiconductor. Science 301(5635):943–945
127. Tartaj P, Morales MP, Veintemillas-Verdaguer S, González-Carreño T, Serna CJ (2003) The preparation of magnetic nanoparticles for applications in biomedicine. J Phys D Appl Phys 36 (13):R182–R197
128. Pankhurst QA (2006) Nanomagnetic medical sensors and treatment methodologies. BT Technol J 24(3):33–38
129. Villanueva A, Cañete M, Roca AG, Calero M, Veintemillas-Verdaguer S, Serna CJ, Morales MP, Miranda R (2009) The influence of surface functionalization on the enhanced internalization of magnetic nanoparticles in cancer cells. Nanotechnology 20(11):115103
130. Mahmoudi M, Sant S, Wang B, Laurent S, Sen T (2011) Superparamagnetic iron oxide nanoparticles (SPIONs): development, surface modification and applications in chemotherapy. Adv Drug Deliv Rev 63(1–2):24–46
131. Safarikova M, Safarik I (1999) Magnetic solid-phase extraction. J Magn Magn Mater 194(1–3):108–112
132. Shinkai M (2002) Functional magnetic particles for medical application. J Biosci Bioeng 94 (6):606–613
133. Yoza B, Matsumoto M, Matsunaga T (2002) DNA extraction using modified bacterial magnetic particles in the presence of amino silane compound. J Biotechnol 94(3):217–224
134. Nam JM, Thaxton CS, Mirkin CA (2003) Nanoparticle-based bio-bar codes for the ultrasensitive detection of proteins. Science 301(5641):1884–1886
135. Rheinländer T, Kötitz R, Weitschies W, Semmler W (2000) Magnetic fractionation of magnetic fluids. J Magn Magn Mater 219(2):219–228
136. Romanus E, Huckel M, Gross C, Prass S, Weitschies W, Brauer R, Weber P (2002) Magnetic nanoparticle relaxation measurement as a novel tool for in vivo diagnostics. J Magn Magn Mater 252(1–3):387–389
137. Kim KW, Ha HK (2003) MRI for small bowel diseases. Semin Ultrasound CT MRI 24 (5):387–402
138. Richardson JC, Bowtell RW, Mader K, Melia CD (2005) Pharmaceutical applications of magnetic resonance imaging (MRI). Adv Drug Deliv Rev 57(8):1191–1209
139. Coroiu I (1999) Relaxivities of different superparamagnetic particles for application in NMR tomography. J Magn Magn Mater 201:449–452
140. Babes L, Denizot B, Tanguy G, Le Jeune JJ, Jallet P (1999) Synthesis of iron oxide nanoparticles used as MRI contrast agents: a parametric study. J Colloid Interface Sci 212 (2):474–482
141. Kim DK, Zhang Y, Kehr J, Klason T, Bjelke B, Muhammed M (2001) Characterization and MRI study of surfactant-coated superparamagnetic nanoparticles administered into the rat brain. J Magn Magn Mater 225(1–2):256–261

142. Harisinghani MG, Barentsz J, Hahn PF, Deserno WM, Tabatabaei S, van de Kaa CH, de la Rosette J, Weissleder R (2003) Noninvasive detection of clinically occult lymph-node metastases in prostate cancer. N Engl J Med 348(25):2491–2499
143. Bjornerud A, Johansson L (2004) The utility of superparamagnetic contrast agents in MRI: theoretical consideration and applications in the cardiovascular system. NMR Biomed 17 (7):465–477
144. Jordan A, Scholz R, Wust P, Fahling H, Felix R (1999) Magnetic fluid hyperthermia (MFH): cancer treatment with AC magnetic field induced excitation of biocompatible superparamagnetic nanoparticles. J Magn Magn Mater 201:413–419
145. Andra W, d'Ambly CG, Hergt R, Hilger I, Kaiser WA (1999) Temperature distribution as function of time around a small spherical heat source of local magnetic hyperthermia. J Magn Magn Mater 194(1–3):197–203
146. Hilger I, Hergt R, Kaiser WA (2000) Effects of magnetic thermoablation in muscle tissue using iron oxide particles—an in vitro study. Invest Radiol 35(3):170–179
147. Wust P, Hildebrandt B, Sreenivasa G, Rau B, Gellermann J, Riess H, Felix R, Schlag PM (2002) Hyperthermia in combined treatment of cancer. Lancet Oncol 3(8):487–497
148. Pardoe H, Clark PR, St Pierre TG, Moroz P, Jones SK (2003) A magnetic resonance imaging based method for measurement of tissue iron concentration in liver arterially embolized with ferrimagnetic particles designed for magnetic hyperthermia treatment of tumors. Magn Reson Imaging 21(5):483–488
149. Mornet S, Vasseur S, Grasset F, Duguet E (2004) Magnetic nanoparticle design for medical diagnosis and therapy. J Mater Chem 14(14):2161–2175
150. Lübbe AS, Bergemann C, Riess H, Schriever F, Reichardt P, Possinger K et al (1996) Clinical experiences with magnetic drug targeting: a phase I study with 4′-epidoxorubicin in 14 patients with advanced solid tumors. Cancer Res 56(20):4686–4693
151. Bonadonna G, Gianni L, Santoro A, Bonfante V, Bidoli P, Casali P, Demicheli R, Valagussa P (1993) Drugs 10 years later—epirubicin. Ann Oncol 4(5):359–369
152. Lübbe AS, Bergemann C, Brock J, McClure DG (1999) Physiological aspects in magnetic drug-targeting. J Magn Magn Mater 194(1–3):149–155
153. Frey NA, Peng S, Cheng K, Sun S (2009) Magnetic nanoparticles: synthesis, functionalization, and applications in bioimaging and magnetic energy storage. Chem Soc Rev 38 (9):2532–2542